1998

A Computational Study on the Dynamic Stall of a Flapping Airfoil

Tuncer, Ismail; Walz, Ralf; Platzer, Max F.

American Institute of Aeronautics and Astronautics, Inc.

Tuncer, Ismail H., Ralf Walz, and Max F. Platzer. "A computational study on the dynamic stall of a flapping airfoil." AIAA paper 2519 (1998): 1998.
https://hdl.handle.net/10945/50285

A98-32420

AIAA-98-2519

A COMPUTATIONAL STUDY ON THE DYNAMIC STALL OF A FLAPPING AIRFOIL

Ismail H.Tuncer *
Middle East Technical University
06531 Ankara, Turkey

Ralf Walz †
Technical University of Karlsruhe
D-76128 Karlsruhe, Germany

Max F. Platzer ‡
Naval Postgraduate School
Monterey, California 93943

Abstract

The dynamic stall boundaries of a NACA 0012 airfoil oscillating in either the pure plunge mode or in the combined pitch and plunge mode is computed using a thin-layer Navier-Stokes solver. Unsteady flowfields are computed at the free-stream Mach number of 0.3, the Reynolds number of $1 \cdot 10^6$, and the Baldwin-Lomax turbulence model is employed. It is found that the pure plunge oscillation leads to dynamic stall as soon as the non-dimensional plunge velocity exceeds the approximate value of 0.35. In addition, the power extraction capability of the airfoil operating in the wingmill mode is studied by computing the dynamic stall boundary for a combined pitch and plunge motion at the reduced frequency values of 0.1, 0.25 and 0.5.

Nomenclature

c	Airfoil chord length (reference length)
h	Plunge amplitude normalized with c
k	Reduced frequency ($\omega c/V_\infty$)
V_∞	Free-stream speed (reference speed)
α_0	Pitch amplitude
ω	Circular frequency of oscillation
ϕ	Phase shift
τ	Non-dimensional time

Introduction

The problem of dynamic stall on helicopter, propeller and wind turbine blades has received considerable attention for quite some time because of the impact of dynamic stall on the blade performance and on the (possibly destructive) loads caused by the dynamic stall phenomenon. The blade is assumed to execute a pitching oscillation about some pitch axis located on the blade chordline. In recent years, a significant amount of new experimental information has been obtained by Chandrasekhara and Carr and by Lorber and Carta. For a comprehensive review of this experimental data we refer to the review paper by Carr and Chandrasekhara [1]. Also, the rapid advances in computational fluid dynamics have made it possible to apply numerical solution techniques of the Reynolds averaged Navier-Stokes equations to this problem. For a review of the current status of dynamic stall computations refer to Ekaterinaris and Platzer [2].

The case of sinusoidal plunge oscillation has received much less attention in past years because a pure plunge oscillation was thought to have much less importance in practical applications. However, it has been known for many years that a flapping wing generates a thrust force. This effect can be predicted using inviscid, incompressible flow theory. For example, Garrick [3] used Theodorson's oscillatory thin-airfoil theory and Platzer et al [4] applied an unsteady panel code to this problem.

Very recently, it has been recognized that flapping wing propulsion may be more efficient than conventional propellers if applied to very small scale vehicles, so-called micro-air vehicles, because of the very small Reynolds number encountered on such vehicles. For this reason, an experimental and computational research program is in progress by the authors to investigate the propulsive characteristics of flapping airfoils. Of special interest is the determination of the dependence of the thrust force on the amplitude and frequency of oscillation and on the flow Reynolds number, especially the combination of these parameters which leads to dynamic stall and therefore loss of thrust and propulsive efficiency.

Another problem of potential practical interest is the extraction of power from an air or water stream by an airfoil which has the plunge and pitch degrees of freedom. As is well known, this combined motion may easily lead to explosive bending-torsion wing flutter. However, as demonstrated by McKinney and DeLaurier [5], the fluttering airfoil can be used as an oscillating-wing windmill (wingmill) for power generation. Here again it will be

*Assistant Professor, Department of Aeronautical Engineering
†Graduate Student, Institut für Strömungslehre
‡Professor, Department of Aero/Astronautics

useful to identify the dynamic stall boundary which limits the generating capacity of the wingmill.

For these reasons it is the objective of this investigation to identify the dynamic stall boundary of a NACA 0012 airfoil which has either the pure plunge or the combined pitch/plunge degrees of freedom. Recent water tunnel flow visualization experiments by Jones et al [6] and Lai et al [7] have provided a considerable amount of information about the flow characteristics of sinusoidally plunging airfoils, but these experiments were largely limited to the visualization and measurement of the wake characteristics. Also, Tuncer and Platzer [8] explored the effect of plunge amplitude on the thrust of a sinusoidally plunging airfoil using a compressible thin-layer Navier-Stokes solver, but they did not consider flows undergoing dynamic stall. In the present paper the same Navier-Stokes solver is applied to the determination of the dynamic stall boundary of the NACA 0012 airfoil at low subsonic Mach numbers. Inviscid panel code solutions are also compared with the Navier-Stokes solutions for attached flows.

Numerical Method

A compressible, thin-layer Navier-Stokes solver is employed for computing the flow over a plunging or pitching and plunging airfoil. The flowfields are analyzed in terms of instantaneous velocity fields and the aerodynamic loads based on the surface pressure distribution. A panel code with wake vortices is also employed.

Navier-Stokes solver

The strong conservation-law form of the 2-D, thin-layer, Reynolds averaged Navier-Stokes equations is solved using an approximately factored, implicit algorithm. The convective terms are evaluated using the third order accurate Osher's upwind biased flux difference splitting scheme. The governing equations in a curvilinear coordinate system, (ξ, ζ), are given as follows:

$$\partial_t \hat{\mathbf{Q}} + \partial_\xi \hat{\mathbf{F}} + \partial_\zeta \hat{\mathbf{G}} = Re^{-1} \partial_\zeta \hat{\mathbf{S}} \qquad (1)$$

where $\hat{\mathbf{Q}}$ is the vector of conservative variables, $(\rho, \rho u, \rho w, e)$, $\hat{\mathbf{F}}$ and $\hat{\mathbf{G}}$ are the inviscid flux vectors, and $\hat{\mathbf{S}}$ is the thin layer approximation of the viscous fluxes in the ζ direction normal to the airfoil surface. The pressure is related to density and total energy through the equation of state for an ideal gas, $p = (\gamma - 1)\left[e - \rho(u^2 + w^2)/2\right]$.

A fully turbulent flow is assumed to exist which is modeled by the Baldwin-Lomax turbulence model.

Computational Domain

The computational domain around the airfoil is discretized with a single C-grid. The plunging or pitching motion of the airfoil is implemented by moving the airfoil and the computational grid as specified by the pitch and the plunge motions:

$$\alpha = -\alpha_0 \cos(kt + \phi)$$
$$y_{pl} = -h \cos(kt) \qquad (2)$$

where α_0 denotes the pitch amplitude, h the plunge amplitude (normalized with the airfoil chord), and ϕ the phase angle between the pitch and plunge motion. A phase angle of $\phi = 90°$ therefore means, that the pitch motion leads the plunge motion by 90 degrees. k is the reduced frequency, defined by $k = \omega c / V_\infty$. Here ω is the circular frequency, c the chord length and V_∞ the free-stream velocity.

Boundary Conditions

Boundary conditions are applied on the airfoil surface and at the farfield boundaries. On the airfoil boundary the no-slip boundary condition is applied, and the density and pressure gradients are set to zero. The surface fluid velocity is set equal to the prescribed local airfoil velocity. At the farfield inflow and outflow boundaries the flow variables are evaluated using the zero order Riemann invariant extrapolation. Further details are described by Tuncer and Platzer [8].

Panel code

In the potential flow solution, UPOT, the flowfield is assumed to be inviscid, irrotational and incompressible. The unsteady flowfield is represented by distributed source and vortex sheets on the airfoil surface and concentrated vortices in the wake. As the unsteady flow solution marches in time, a vortex is shed from the trailing edge of the airfoil and convected downstream with the local velocity. The velocity field is expressed in terms of a disturbance potential. Laplace's equation is then solved for the disturbance potential by superimposing the source/sink and vorticity singularity solutions to satisfy the boundary condition on the airfoil surface. A more detailed description is given by Platzer et al [4].

Results

We first computed flowfields as a NACA0012 airfoil undergoes a pure plunge oscillation at various amplitudes and reduced frequencies, and then computed the flowfields for combined pitch and plunge motions. The flowfields were mostly computed at the free-stream Mach

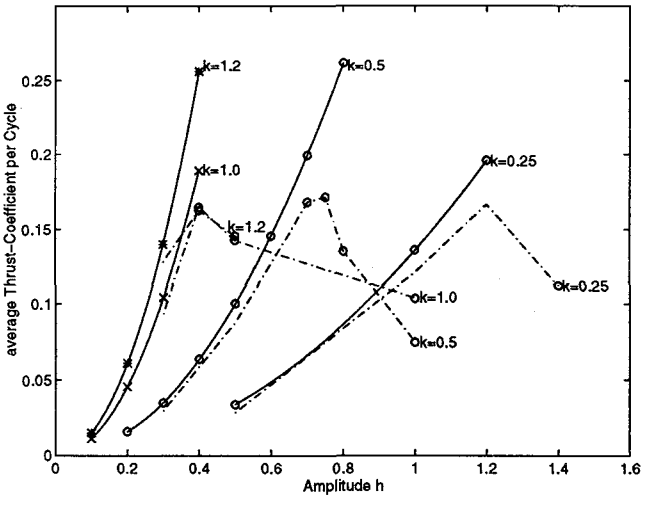

Fig. 1 Thrust coefficient versus amplitude for low reduced frequencies, $k = 0.25 - 1.2$

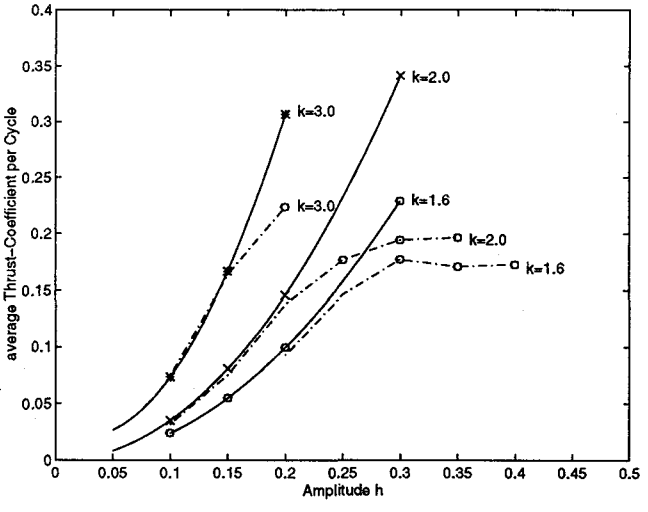

Fig. 2 Thrust coefficient versus amplitude for high reduced frequencies, $k = 1.6 - 3.0$

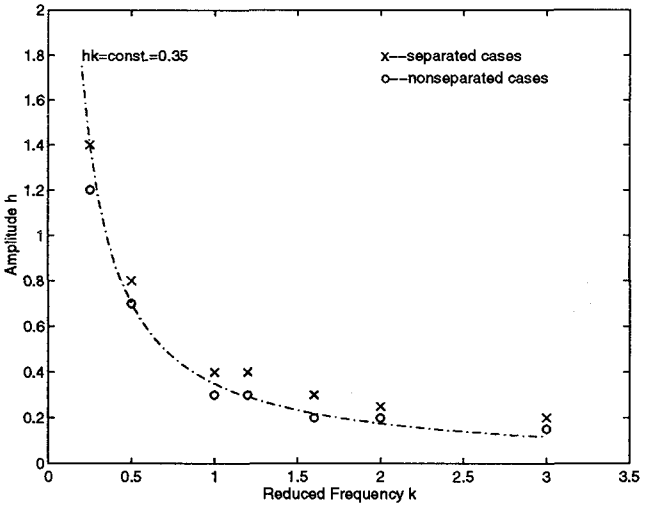

Fig. 3 Flow separation versus $hk = 0.35$

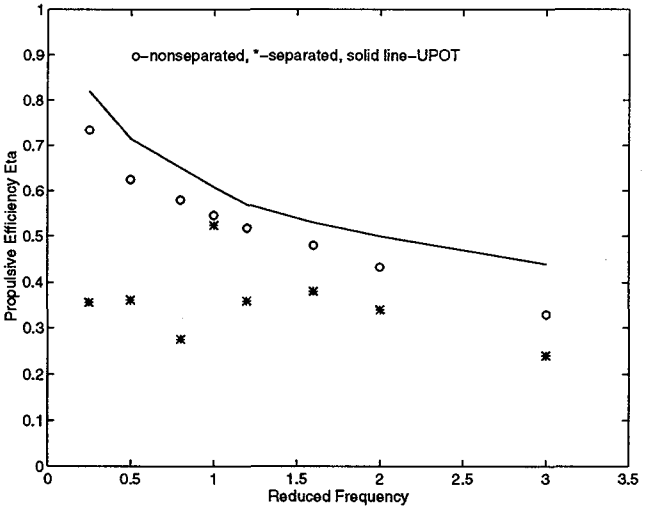

Fig. 4 Propulsive efficiency for attached and separated flows.

number of $M = 0.3$ and the Reynolds number of $Re = 1 \cdot 10^6$, which is based on the airfoil chord. Additional computations were also performed for a Reynolds number of $5 \cdot 10^6$. However, no significant differences in the flowfields were observed. The Navier-Stokes solutions were obtained on a C-type grid, which is of 121x62 size. A grid study with 241x61, 241x91 and 311x71 size grids showed that the computed results were not sensitive to the grid size. In the panel code solutions 75 panels were employed on the airfoil surface.

Pure Plunge Oscillation

In Figures 1 and 2, the results of thrust computations for the harmonically plunging NACA 0012 airfoil are shown. The reduced frequency, based on the airfoil chord, was varied between 0.25 and 3.0 and the non-dimensional plunge amplitude, based on the airfoil chord, ranged between 0.1 and 1.4. For a given reduced frequency, the amplitude was gradually increased until the combination of frequency and amplitude which produced the maximum thrust could be identified. In the lower reduced frequency range, shown in Figure 1, the thrust is observed to decrease quite rapidly as soon as a sufficient amount of dynamic stall is encountered. It can also be seen, that the Navier-Stokes predictions are in good agreement with the incompressible potential flow prediction up to the dynamic stall onset point, using the panel code. At higher reduced frequencies, shown in Figure 2, the onset of dynamic stall has a much more benign effect on the achievable maximum thrust. Indeed, it is seen that the thrust still increases after encountering dynamic

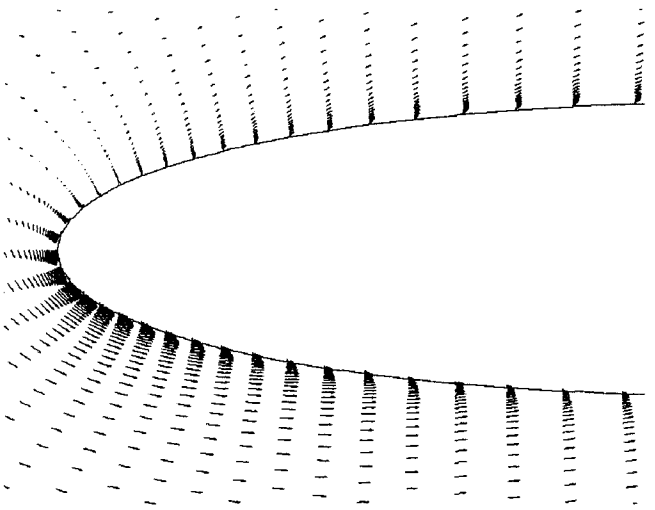

Fig. 5 Attached Flow, $k = 0.8, h = 0.4$

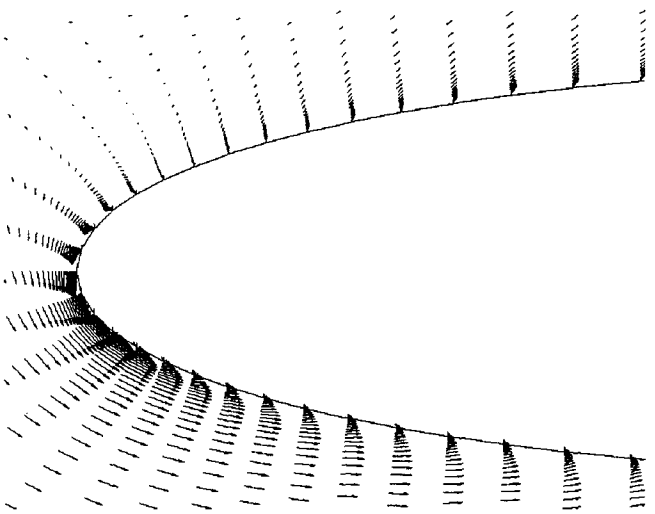

Fig. 6 Onset of flow separation, $k = 0.8, h = 0.5$

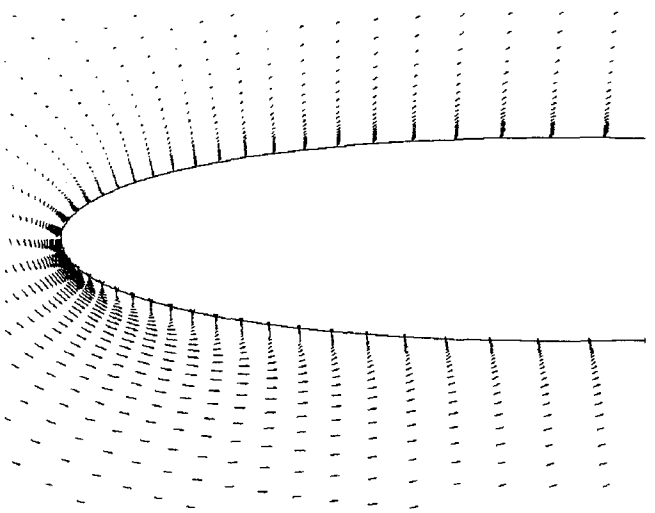

Fig. 7 Light flow separation, $k = 0.8, h = 0.6$

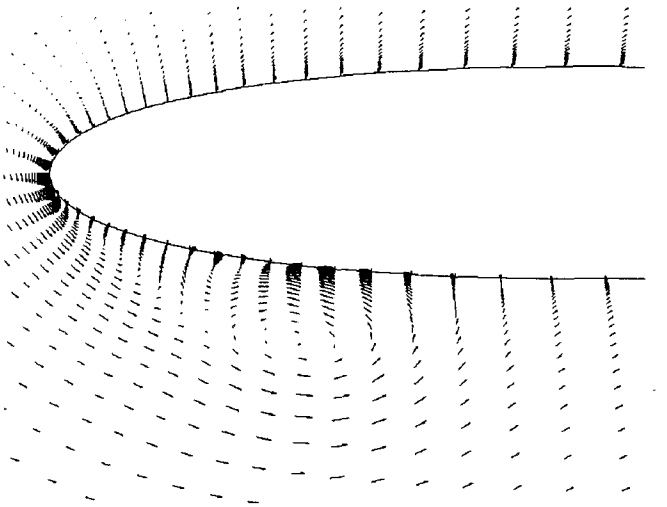

Fig. 8 Fully separated flow, $k = 0.8, h = 0.7$

stall and then remains fairly constant with increasing amplitude. Again, the Navier-Stokes and the inviscid flow predictions agree at lower plunge amplitudes where the flow remains attached over the complete oscillation cycle.

If one plots the dynamic stall onset points one obtains the stall boundary shown in Figure 3. Evidently, the maximum achievable thrust is a function of the product of reduced frequency and amplitude hk. This product merely represents the maximum non-dimensional plunge velocity. One can either choose to select a large amplitude and a small frequency or vice versa, but as soon as the product exceeds a critical value, dynamic stall is encountered which limits the achievable thrust. On the other hand, if one wants to optimize the propulsive efficiency it is advantageous to operate in the low frequency/large amplitude range as shown in Figure 4. Here the panel code prediction is shown as the solid line. The open circles and the starred symbols indicate the Navier-Stokes predicted efficiencies for cases just before and after the occurrence of the dynamic stall, corresponding to the cases shown in Figure 3. It is seen that the efficiency drops rapidly, in particular in the low frequency range. The dynamic stall mostly occurs when the airfoil passes through the zero amplitude position because it then experiences the maximum incidence angle.

Figures 5-8 show the velocity field around the leading edge when the airfoil passes the mean position during the upstroke, as the plunge amplitude changes from 0.4 to 0.7 at a constant reduced frequency of $k = 0.8$. It is seen that at $h = 0.4$ the flow is still fully attached, but increasing amounts of flow separation are observed as the plunge amplitude increases. Additional details are given by Walz in Reference 12.

Thrust-Producing Pitch/Plunge Oscillation

If the airfoil is set into a combined pitch and plunge motion, one has to pay attention to the effective angle of attack the airfoil experiences. As discussed by Jones and Platzer [9], for small pitch amplitudes, corresponding to Figure 9a, thrust is produced whereas at higher pitch amplitudes, corresponding to Figure 9b, drag is produced and power is extracted from the flow.

The thrust coefficient and the propulsive efficiency of a NACA 0012 airfoil whose combined pitch oscillation about the mid-chord leads the plunge oscillation by a phase angle ϕ (which varies from 30 to 150 degrees) is given in Figures 10 and 11. This case was recently investigated by Isogai et al [10] for a Reynolds number of $1 \cdot 10^5$ using a Navier-Stokes solver in combination with a Baldwin-Lomax turbulence model. As can be seen from Figure 10, the non-dimensional plunge amplitude is 1 and the pitch amplitude is 10°. This corresponds to a thrust producing case, Figure 9a. To facilitate a direct comparison with Isogai et al [10] the plunge amplitude and the reduced frequency are based on the half-chord and the thrust coefficient is defined as

$$C_T = \frac{Thrust}{\left(\frac{1}{2}\rho V_\infty^2 (kh)^2 c\right)}$$

and the computations were performed at the Reynolds number of 10^5.

The two Navier-Stokes computations are in qualitative agreement, but the large differences in the predicted values at $k = 0.15$ require further investigation. Similar qualitative trends are observed for the propulsive efficiency shown in Figure 11, but significant quantitative differences are again found for $k = 0.15$.

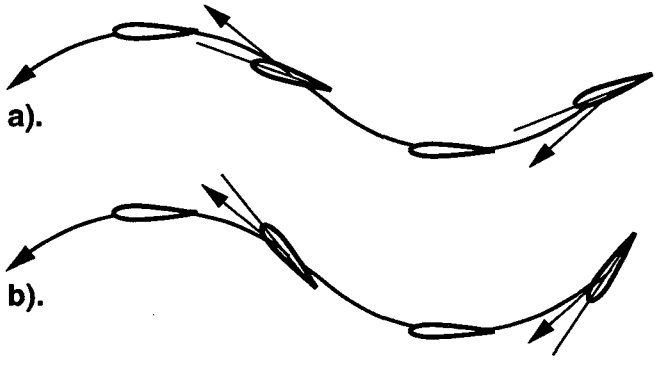

Fig. 9 Combined pitch/plunge oscillation with a) a small and b) a large pitch amplitude

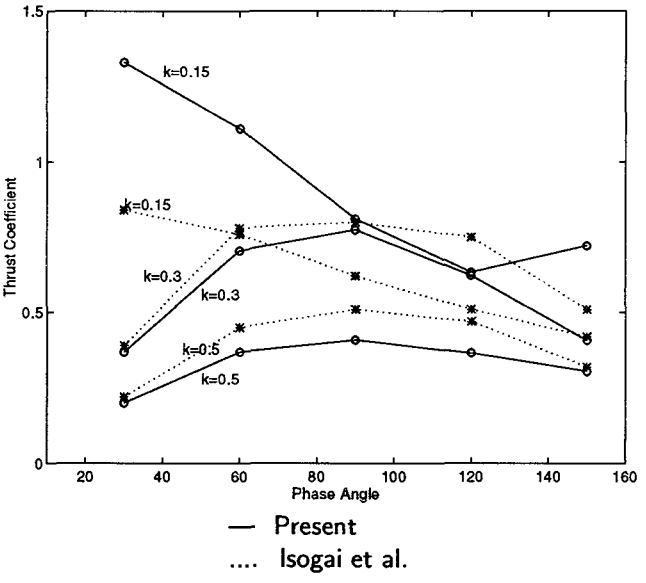

Fig. 10 Thrust coefficient versus phase angle at $h = 1.0, \alpha_0 = 10°$, $Re = 1 \cdot 10^5$

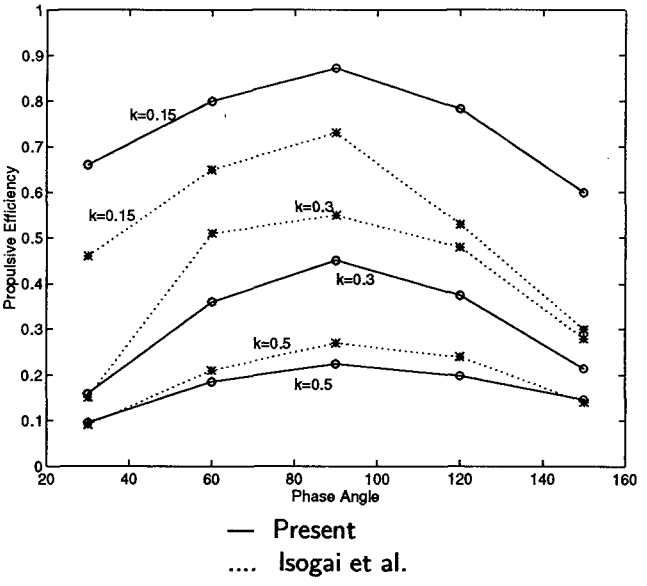

Fig. 11 Propulsive efficiency versus phase angle at $h = 1.0, \alpha_0 = 10°$, $Re = 1 \cdot 10^5$

Power-Producing Pitch/Plunge Oscillation

An increase of the pitch amplitude eventually leads to a sign change of the effective angle of attack. The airfoil motion now occurs as shown in Figure 9b. As pointed out for example by Duncan [11], the airfoil now is able to extract energy out of the airstream which may cause explosive airfoil bending-torsion flutter. Therefore, an airfoil which is forced to oscillate in such a pitch and plunge mode will run under its own power, i.e., as a flutter engine, when the phase difference between pitch and plunge

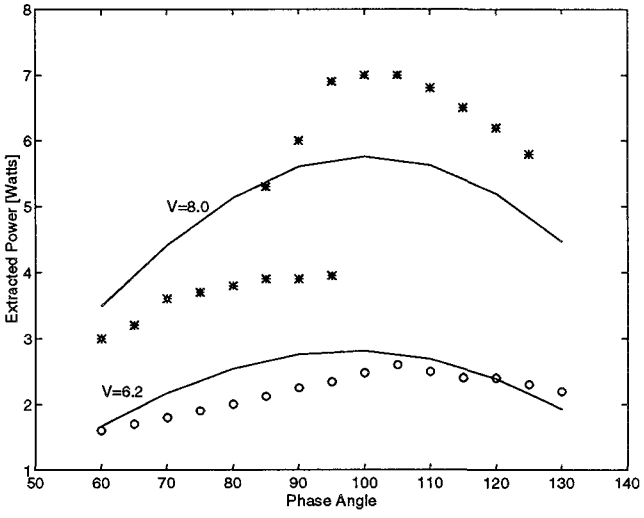

— UPOT,
o Experiment at $V_\infty = 6.2m/sec$,
* Experiment at $V_\infty = 8.0m/sec$

Fig. 12 Comparison of computed power of experiment of McKinney & DeLaurier, Plunge amplitude = 0.3, pitch amplitude = 25°

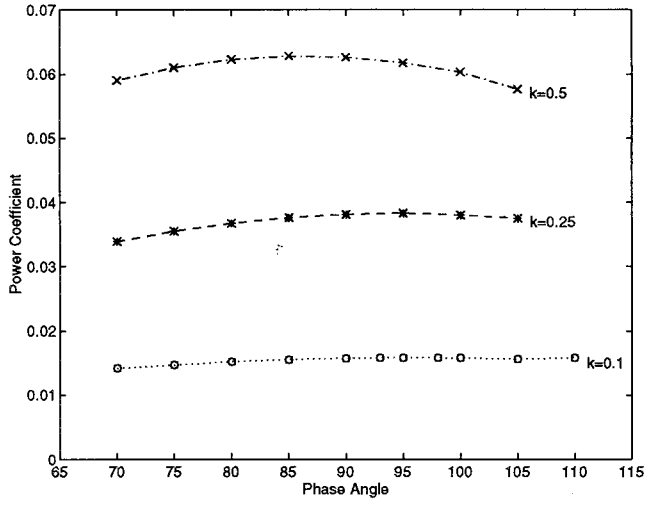

x $\alpha_0 = 16°$
* $\alpha_0 = 20°$
o $\alpha_0 = 24°$

Fig. 13 Computed power coefficient (UPOT) versus phase angle; plunge amplitude $h = 0.2$.

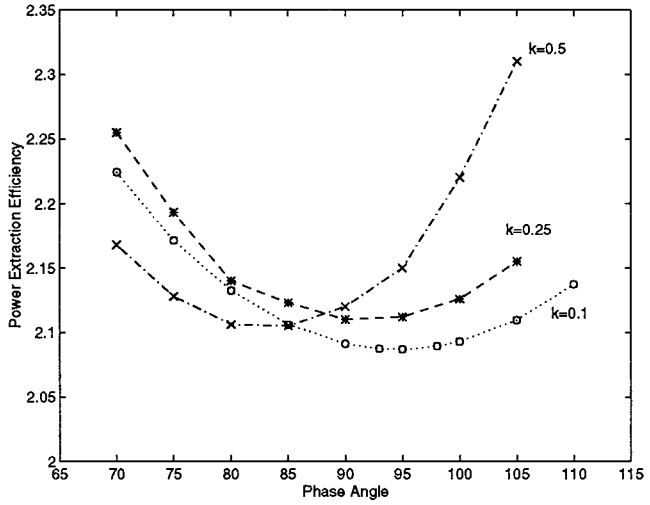

x $\alpha_0 = 16°$
* $\alpha_0 = 20°$
o $\alpha_0 = 24°$

Fig. 14 Propulsive efficiency (UPOT) versus phase angle; plunge amplitude $h = 0.2$

is close to 90 degrees or a smaller angle down to about 15 degrees, but it will stop when the phase difference is reduced to zero. McKinney and DeLaurier [5] explored the feasibility of using such an oscillating-wing windmill (wing-mill) for power generation. Using an airfoil which oscillated with a pitch amplitude of 25 degrees and a non-dimensional plunge amplitude of 0.3 they measured the power values shown in Figure 12. These experimental data are affected by the occurrence of dynamic stall, especially at the higher wind speed of 8 m/sec. Nevertheless, the inviscid panel code predictions agree reasonably well with the measured power values.

As in the case of thrust production, it is of interest to explore the conditions for maximum power extraction. Figure 13 shows the dependence of power coefficient on reduced frequency, pitch amplitude and phase angle between pitch and plunge for a NACA 0012 airfoil which is oscillating in plunge with a non-dimensional plunge amplitude of 0.2. These results are based on the inviscid panel code. To determine the stall boundary at a phase angle of 100 degrees the computations were repeated with the Navier-Stokes code. For the three reduced frequencies shown on Figure 13, the Navier-Stokes calculations predicted no flow separation, but an increase of the pitch amplitude by 2 degrees produced the onset of dynamic stall in each case. Therefore, the curves shown in Figure 13 can be regarded as the wingmill operating lines close to stall. It should be noted that the maximum effective angle of attack is approximately the same for each combination of reduced frequency and pitch amplitude, because the angle of attack induced by the plunge motion increases with increased reduced frequency. If the induced angle of attack due to the plunging motion, α_i, is considered as

$$\alpha_i = \arctan(hk)$$

one obtains the following effective angles of attack, α_e:

- $k = 0.5 \quad \alpha_e = \alpha - \alpha_i = 24 - 5.7 = 18.3$
- $k = 0.2 \quad \alpha_e = \alpha - \alpha_i = 20 - 2.9 = 17.1$
- $k = 0.1 \quad \alpha_e = \alpha - \alpha_i = 16 - 1.2 = 14.8$

Hence, the effective angles of attack are in a range of values where one expects the onset of flow separation. This consideration provides a plausible explanation for the occurrence of stall predicted by the Navier-Stokes code. It can also be seen that the maximum power extraction occurs at phase angles between 80 and 110 degrees. This is consistent with the experimental findings of McKinney and DeLaurier. Finally, in Figure 14 the panel code computed power extraction efficiencies are plotted for the same parameter combinations shown in Figure 13. For simplicity, the efficiency is defined here as the inverse value of the propulsive efficiency. This is in contrast to the efficiency definition used by McKinney and DeLaurier. Therefore, efficiency values greater than one are obtained, where a "low value" corresponds to a high efficiency. It is seen that a wingmill running at a reduced frequency of 0.1 has a slightly better efficiency than one running at a higher frequency. Again, the highest efficiencies occur at phase angles between 80 to 110 degrees.

Concluding Remarks

Thin-layer Navier-Stokes computations were performed for low subsonic flow over a NACA 0012 airfoil oscillating in either the pure plunge or the combined pitch/plunge mode. Parametric variation of the frequency and amplitude of the pure plunge oscillation showed that dynamic stall is encountered as soon as the non-dimensional plunge velocity hk exceeds values close to 0.35. Additional calculations were performed for three reduced frequency values 0.1, 0.25 and 0.5 to determine the maximum power of a NACA 0012 airfoil which operates as a wingmill. Further studies are necessary to explore the more precise nature of the dynamic stall behavior of plunging and pitching/plunging airfoils over a wider range of Mach and Reynolds numbers. To this end, the computations need to be repeated with higher order turbulence models and a proper transition model.

Acknowledgments

This investigation was supported by the Naval Research Laboratory, project monitor Kevin Ailinger. Also, the authors gratefully acknowledge the assistance of Dr. Kevin Jones.

References

1. Carr, L.W. and Chandrasekhara, M.S., "Compressibility Effects on Dynamic Stall", Progress in Aerospace Sciences , 32, 523-573, 1996

2. Ekaterinaris, J.A. and Platzer, M.F., "Computational Prediction of Airfoil Dynamic Stall", Progress in Aerospace Sciences, 33, 1998, (to be published)

3. Garrick, I.E., "Propulsion of a Flapping and Oscillating Airfoil", NACA TR-567, 1937

4. Platzer, M.F., Neace, K.S., Pang, C.K., "Aerodynamic Analysis of Flapping Wing Propulsion", AIAA paper No. 93-0 484, January 1993

5. McKinney, W. and DeLaurier, J., "The Wingmill: An Oscillating-Wing Windmill", Journal of Energy, Vol. 5, No. 2, 109-115, March-April 1981

6. Jones, K.D., Dohring, C.M., Platzer, M.F., "Wake Structures Behind Plunging Airfoils: A Comparison of Numerical and Experimental Results", AIAA paper No. 96-0078, January 1996

7. Lai, J.C.S., Yue J., Platzer, M.F., "Control of Backward Facing Step Flow Using a Flapping Airfoil", ASME Fluids Engineering Division Summer Meeting, FEDSM97-3307, June 1997

8. Tuncer, I.H. and Platzer, M.F., "Thrust Generation due to Airfoil Flapping", AIAA Journal, Vol. 34, No. 2, 324- 331, February 1996

9. Jones, K.D. and Platzer, M.F., "Numerical Computation of Flapping Wing Propulsion and Power Extraction", AIAA Paper No. 97-0826, January 1997

10. Isogai, K., Shinmoto, Y., Watanabe, Y., "Effects of Dynamic Stall Phenomena on Propulsive Efficiency and Thrust of a Flapping Airfoil", AIAA Paper No. 97-1926, June 1997

11. Duncan, W.J.,"Introductory Survey", AGARD Manual on Aeroelasticity, Vol. I

12. Walz R., "A Computational Investigation of the Dynamic Stall Boundaries of the NACA 0012 Airfoil Oscillating in Pure Plunge or in the Combination Pitch/Plunge Mode", TU Karlsruhe, June 1998